Supplemental figure legends

Figure S1 **Case-by-case analysis of gains and losses across chromosome 6q in follicular lymphomas.** Related to Figure 1. **A,** Regions of copy number loss are indicated in blue, gains in red, color intensity represents the signal strength, and aligned to a map of chromosome 6 with indication of CRD4 and CRD9. The location of some key genes is indicated; **B,** *EPHA7* is affected by 8/13 deletions involving CDR4; similarly *TNFAIP3* is affected by 9/12 cases harboring CDR9 deletions**; C**, Diagram indicating the deletion of *EPHA7* and *TNFAIP3* in individual cases. All deletions are almost entirely hemizygous and no gene is directly affected by bi-allelic loss.

Figure S2 **Individual validation of the screen results and characterization of EphA7 shRNAs.** Related to Figure 2. **A,** FL5-12/Bcl2 cells partially transduced with indicated shRNA/GFP or control constructs are shifted into IL3-deficient media and monitored for changes in the proportion of GFP expressing cells. Positive results implicate these genes in survival and proliferation of Bcl2 expressing B-cell upon IL-3 depletion, a negative result does not rule out other functions that are not assessed in this assay; **B**, Assessment of three additional shRNAs (sh2-4) against *EphA7* in FL5-12 cells; **C**, Immunoblot on lysates of FACS sorted FL5-12 cells expressing three shRNAs against *EphA7* (sh2-4) or vector (V) and probed as indicated (p21 has been reported as a common off-target of shRNAs; **D** FACS analysis showing enrichment of FL5-12 cells transduced with the shRNA against murine EphA7/GFP and in the presence of empty vector but not in the presence of the human *EPHA7* cDNA/RFP; **E**, Cell cycle analysis of FL5-12 cells

transduced with vector or shRNA against *EphA7* analyzed at different times before and after IL-3 withdrawal and re-addition.

Figure S3 **Molecular characterization of murine *vavPBcl2* lymphomas.** Related to Figure 3 **A,** Immunoblot on lysates from *vavPBcl2* transgenic HSCs and splenocytes probed for EphA7; **B**, Enrichment of two independent *EphA7* shRNAs (sh1 and sh4) during lymphoma development *in vivo* (subsequent experiment were performed with sh1 against EphA7); **C**, Annotation indicating the location of primers used in the clonality analysis; **D**, Nested PCR analysis of DJ recombination reveals a single band at ~ 140bp and indicates clonality of vavPBcl2/EphA7 lymphoma; **E,** PCR analysis of lymphomas arising in transgenic vavPBcl2 animals and in mice receiving HSCs transduced with the indicated constructs confirms their clonality.

Figure S4. **EPHA7 expression and methylation analyses.** Related to Figure 4. **A,** Loss of EPHA7 expression in human FL is significantly associated with higher tumor grade; **B,** Micrographs representing the different scoring criteria of EPHA7 expression by immunohistochemisty; **C**, Quantification of the Mass-array for *EPHA7* promoter methylation analysis; **D**, Quantification of *EPHA7* promoter methylation in GC-B-cells and FL and DLBCL for two independent probes; **E**, Quantification of *EPHA7* promoter methylation in GC-B-cells and 24 human lymphoma cell lines for two independent probes; **F**, RT-PCR showing re-expression of the truncated *EPHA7* transcript in SU-DHL-10 cells upon treatment with 1 and 5µg 5'aza-2'-deoxycytidine (Aza); **G**, Domain structure; **H**, Predicted three-dimensional structure based on similarity with the known

EPHA2 structure; **I**, Gel purification of the FC-tagged, ectodomains of EPHA7 ($EPHA7^{FC}$).

Figure S5 **Mechanistic studies on EPHA7 signaling.** Related to Figure 5. **A**, Detection of the EPHA7 protein in the serum of healthy volunteers by ELISA compared to PBS as negative control (NEG); **B**, EPHA2 expression in Raji cells by immunoblot; **C,** Immunoprecipitation of lysates from DoHH2 cells treated with $EPHA7^{FC}$ (FC-tagged ectodomain of EPHA7) or FC, IP with anti-EPHA7 and probed against EPHA7 and EPHA2; **D,** Immunoblot on cell lysates of DHL-6, DoHH2, and Karpas422 cells treated with increasing amounts of $EPHA7^{FC}$; **E**, Immunoblot on lysates of Raji cells treated with an siRNA against EPHA2 for the indicated times and probed as indicated; **F**, FL5-12/Bcl2 cells expressing vector or shEphA7 are probed with the indicated antibodies; **G**, Immunoblot on FL5-12 cells expressing the indicated *EphA7* shRNAs probed for ERK phosphorylation; **H**, Lysates on FL5-12 cells expressing an shRNA against murine *EphA7* and either vector or the human *EPHA7* that is not a target of the shRNA; **I**, FL5-12/Bcl2 cells expressing the shEphA7 (FL5-12/Bcl2/shEphA7) are treated with $EPHA7^{FC}$ (5 µg/ml) for the indicated times and probed as indicated; **J,** Phospho-protein array probed with lysates from Raji cells that are untreated or treated for 15 minutes with 5 µg/ml purified $EPHA7^{FC}$; **K,** Quantification of phospho-protein array results, the blue line indicates values for untreated cells; **L and M,** Raji (L) and SU-DHL-10 (M) lymphoma cells treated with $EPHA7^{FC}$ as before and probed for the indicated signaling molecules; **N,** Gel shift assay showing interaction of purified EPHA7 protein with EPHA2 and EPHA3, but not with EPHA4; **O,** Expression levels of EPHA2 across normal

tissues and FL samples (other EPHA receptors were not detectable in human FL not shown); **P,** Gel shift assay showing the interaction of purified EPHA7 with ephrins A1, A4 and A5, but not with ephrins A2 or A3; **Q**, Expression of ephrin A3 in normal tissues and FL samples (we also find expression of ephrin A1, but not ephrins A2, A4, or A5 not shown); **R**, Site-directed mutagenesis to create a mutation in the ligand binding domain (T105Q) that disables EPHA7 binding to ephrin ligands; **S and T**, Wild type EPHA7 and EPHA7/T105Q equally reduce ERK activation by immunoblot (S) and inhibit the proliferation of FACS sorted Raji cells (T).

Figure S6 **Functional consequences of EPHA7 re-expression.** Related to Figure 6. **A-C,** Retroviral expression of *EPHA7*^{TR} in human lymphoma cells; **A,** qRT-PCR showing the level of retroviral expression of *EPHA7*^{TR} mRNA in Raji and SU-DHL-10 cells; **B**, Growth curve on FACS sorted populations of vector or *EPHA7*^{TR} expressing Raji and SU-DHL-10 cells; **C**, Progressive depletion of *EPHA7*^{TR}/GFP expressing Raji cells from mixed populations during 72h *in vitro* culture; **D-G**, Induction of apoptosis and tumor remissions by EPHA7^{FC}. **D,** FACS analysis of apoptosis induced by treatment with 5µg EPHA7^{FC} in Raji, Karpas422 and DoHH2 cells; **E,** Quantification of apoptosis assays on a panel of lymphoma lines (V = Vehicle/FC; E7 = EPHA7^{FC}; $p < 0.05$ for all Vehicle vs. EPHA7^{FC}); **F,** Photograph of tumors ex situ following treatment with 20µg EPHA7^{FC} or vehicle (FC); **G,** tumor weights comparing treated and mock treated tumors ($p < 0.05$ for SU-DHL-10 and Raji).

Figure S7 **Characterization of an anti-CD20-EPHA7^{TR} fusion antibody**. Related to Figure 7. **A,** ELISA measurement of anti-CD20 and anti-CD20-EPHA7^{TR} antibody production; **B**, FACS analysis of binding to the CD20+ Raji cells by the anti-CD20 and anti-CD20-EPHA7^{TR} antibodies using and a FITC labeled anti-IgG antibody; **C**, ELISA assay for EPHA2 phosphorylation on Raji cells treated with vehicle (Untr.), EPHA7^{FC} or anti-CD20-EPHA7^{TR} (*p (vehicle vs. either treatment) < 0.05); **D,** Apoptosis of untreated (Untr.), anti-CD20 (CD20) or anti-CD20-EPHA7^{TR} (CD20/E7) treated DoHH2 cells at 24h and 48h; * and ** indicate significant differences between untreated and anti-CD20 and between anti-CD-20 versus anti-CD20-EPHA7^{TR} treated cells, respectively; **E,** Proliferation of DoHH2 cells untreated (Untr), treated with anti-CD20 (CD20), or anti-CD2-EPHA7^{TR} fusion (CD20/E7), * indicates significant delay ($p < 0.05$) between untreated or anti-CD20 treated versus anti-CD20-EPHA7^{TR} treated cells; **F,** Microscopic histology on Raji xenografts. Tumors were either vehicle treated or treated with anti-CD20-EPHA7^{TR} and collected 2h after the last of 5 applications of 1µg of antibody. The anti-CD20-EPHA7^{TR} treated tumors reveal some increase in TUNEL positivity, much reduced proliferation and ERK phosphorylation; **G,** Representative micrographs from necropsies performed as part of toxicity studies. Toxicity studies were performed on 4 animals treated with purified EPHA7FC or anti-CD20/EPHA7 at twice the dose used in therapeutic experiments and analyzed 24h and 7d after treatment. Briefly, no major toxicity was observed, we found modest increases in serum glucose levels; necropsy revealed no organ damage, and blood count showed only a mild decrease in mean corpuscular hemoglobin concentration (MCHC) in the absence of anemia.

Supplemental tables

Table S1 **Detailed analysis of chromosome 6 genomic alterations in follicular lymphoma by array-CGH.** Related to Figure 1

Table S2 **Summary of chromosome 6q deletions in follicular lymphoma.** Related to Figure 1

Table S3 **Genes encompassed by deletions on chromosome 6q in follicular lymphomas.** Related to Figure 1

Table S4 **Short-hairpin RNA sequences included in the 6q-deletion library.** Related to Figure 2

Table S5 **Surface marker analyses of murine *vavPBcl2* lymphomas.** Related to Figure 3

Table S6 **Analysis of vavPBcl2 lymphomas for evidence of somatic hypermutation by direct sequencing.** Related to Figure 3

Table S7 **Summary of human follicular lymphoma tissue microarray (TMA) stains for EPHA7.** Related to Figure 4

Supplemental Experimental procedures

Array-CGH. DNA from fresh frozen tissue or OCT-embedded was isolated by the standard phenol-chloroform extraction method. DNA was quantified using the Nanodrop spectrophotometer, quality assessed by the 260:280 ratios and integrity visualized on a 1% agarose gel with ethidium bromide. Prior to submission to the Genomics core for labeling and hybridization to the Agilent 244K oligonucleotide array, digestion efficiency of each DNA was checked by incubating 1µg of DNA with 1µl of HaeIII (10U/µl) at 37°C for 2 hours and running in parallel, the undigested and digested DNA (100ng each) on a 1% agarose gel along with the 1kb DNA ladder. Human male DNA obtained from Promega (Cat# G147A) served as the reference DNA. Labeling and hybridization was performed according to protocols provided by Agilent. The slides were scanned at 5-µm resolution using the Agilent G2565 Microarray Scanner System and Agilent Feature Extraction software (v9.1) was used to generate the data (Agilent Technologies; http://www.agilent.com).

DNA copy number analysis. All genomic positions described in this study refer to UCSC May 2004 human reference sequence (hg17/NCBI build 35) with the exception of figure 4, which uses hg18/build 36. The modified CBS algorithm was used to identify segmental gains and losses along the autosomes1. Change-points were defined as segments, corresponding to p-values < 0.05. A common region of deletion (CRD) was defined as gain and/or loss of 2 contiguous probes observed in >10% of the cases. A total of 92 CRDs were identified and of these, 4 were physiological changes (B- and T-cell receptors), 50 were copy number variants (CNVs) and the remaining 38 were tumor

specific. The Database of Genomic Variants (DGV), a catalogue of structural variations curated by The Centre for Applied Genomics (TCAG), Toronto, Canada (http://projects.tcag.ca/variation/) was used to identify and exclude CNVs. At the time of data analysis, this catalogue comprised of 8083 entries that mapped to 3933 genomic loci [variation.hg17.v2.txt; September 05, 2007 (Build 35/hg17)]. CGH data was further processed using Agilent's Feature Extraction software to quantitate the images. For normalization we used a custom GC-normalization algorithm, which does a loess norm on both the total intensity of the probes and the local GC content in the genomic region surrounding the probes. The normalized data was segmented using the standard CBS algorithm available from the Bioconductor libraries for R (DNAcopy). Each sample was then normalized to its own per sample noise by dividing the segment means by the derivative noise (the mean absolute values of the difference between adjacent probes on the arrays). The next step used the RAE [Taylor2008] algorithm to do a multi-sample analysis of the entire cohort. The RAE algorithm computes per-sample calibrated thresholds, which can be used to compare signal levels across samples. The threshold function converts the log2 ratio signals from the CBS output via two logistic functions to a loss [-1,0] and gain [0-1] indicator output that is then averaged to give the genome-wide gain/loss recurrence frequency (plotted in figure 1). For the chromosome 6q loss analysis we used global threshold of -0.5 for loss and 4.5 for homozygous deletion.

Molecular analysis of murine tumors. Was determined by nested PCR analysis of DJ recombination on lymphoma DNA as described (Yu and Thomas-Tikhonenko, 2002). The sample was analyzed using Agilent 2100 Bioanalyzer platform (DNA analysis 25-

1000bp: assay class DNA 1000). For DNA extraction frozen tissue was submerged in liquid nitrogen, followed by pulverization. The powder was collected and transferred to the Eppendorf tube on ice. DNA purification was done using the Qiagen Puregene Gentra cell kit (Qiagen, Valencia, CA). DNA was diluted in water and the quality was assessed in 1% agarose gel. **Somatic Hypermutation analysis**. Genomic DNA was extracted from lymphomas in transgenic vavPBcl2 mice and lymphomas from transplanted HSC. DNA samples were amplified as described (McBride et al., 2008). The PCR product was directly sequenced exactly as reported (Mandelbaum et al., 2010).

Gel shift assays. Pull-down experiments were done essentially as described earlier (Himanen et al., 1998). In brief, 5 μg of the recombinant extracellular domain of EphA7 was incubated with Fc-tagged ephrin ectodomains (R&D Systems) at room temperature for 30 min. in 500 μl binding buffer containing 20 mM HEPES (pH 8.2), 150 mM KCl, and 2 mM MgCl2. ProteinA Sepharose Fast Flow beads (GE Healthcare) were washed with the binding buffer, added to the reaction mixture, and shaken (not stirred) at room temperature for 30 min. The beads were then harvested by centrifugation, washed twice with 500 μl of the binding buffer, and the bound proteins were separated on a 10-20% polyacrylamide gel.

Site-directed mutagenesis. Lentiviral vector expressing EphA7^{TR} was mutated T105Q residue by site direct mutagenesis using the QuikChange II XL Site-Directed

Mutagenesis Kit (Agilent). The primer sequences used to mutate the site are EphA7 T105Q: Fwd $^{5'}$AATGCACAAAGG ATTTTTGTAGAATTGAAATTCCAGCTGAGGGATTGTAACAGTC TT$^{3'}$ Rev $^{5'}$AAGACTGTTACAATCCCTCAGCTGGAAT TTCAATTCTACAAAAATCCTTTGTGCATT$^{3'}$.

Toxicity analyses. Four females of C57/Black mice were treated by tail vein injection with 3 mg of purified CD20-Epha7 and 40 mg of EphA7^{FC} purified protein. 1 and 7 days after treatment, blood was collected for hematology and biochemical analysis and the animals were sacrificed and a complete necropsy was performed.

Quantitative DNA methylation analysis was carried out using the Epityper/Massarray system from Sequenom. The Epityper assay is a tool for the detection and quantitative analysis of DNA methylation using base-specific cleavage of bisulfite-treated DNA and Matrix-Assisted Laser Desorption/Ionization Time-of-Flight Mass Spectrometry (MALDI-TOF MS). Specific PCR primers for bisulfite-converted DNA were designed using the EpiDesigner software (www.epidesigner.com), for the entire CpG island of the genes of interest. Primer sequences are available upon request. T7-promoter tags were added to the reverse primer to obtain a product that was *in vitro* transcribed, and a 10-mer tag was added to the forward primer to balance the PCR conditions. One µg of tumor DNA was subjected to bisulfite treatment using the EZ-96 DNA methylation Kit, which results in the conversion of unmethylated cytosines into uracil, following the manufacturer's instructions (Zymo Research). PCR reactions were carried out in duplicate, for each of the 2 selected primer pairs, for a total of 4 replicates per sample. For each replicate, 1 ml of bisulfite-treated DNA was used as template for a 5 ml PCR

reaction in a 384-well microtiter PCR plate, using 0.2 units of Kapa2G Fast HotStart DNA polymerase (Kapa Biosystems, SA), 200 mM dNTPs, and 400 nM of each primer. Cycling conditions were: 94 ^{0}C for 15 minutes, 45 cycles of 94 ^{0}C for 20 seconds, 56 ^{0}C for 30 seconds, 72 ^{0}C for 1 minute, and 1 final cycle at 72 ^{0}C for 3 minutes. Unincorporated dNTPs were deactivated using 0.3 U of shrimp alkaline phosphatase (SAP) in 2 ml, at 37 ^{0}C for 20 minutes, followed by heat inactivation at 85 ^{0}C for 5 minutes. Two ml of SAP-treated reaction were transferred into a fresh 384-well PCR plate, and *in vitro* transcription and T cleavage were carried out in a single 5 ml reaction mix, using the MassCleave kit (Sequenom) containing 1 X T7 polymerase buffer, 3 mM DTT, 0.24 ml of T Cleavage mix, 22 units of T7 RNA and DNA polymerase, and 0.09 mg/ml of RNAseA. The reaction was incubated at 37 ^{0}C for 3 h. After the addition of a cation exchange resin to remove residual salt from the reactions, 10 nl of Epityper reaction product were loaded onto a 384-element SpectroCHIP II array (Sequenom). SpectroCHIPs were analyzed using a Broker Biflex III matrix-assisted laser desorption/ionization–time of flight (MALDI-TOF) mass spectrometer (SpectroREADER, Sequenom). Results were analyzed using the Epityper Analyzer software, and manually inspected for spectra quality and peak quantification. The primer sequences for each gene are available upon request. *In vitro* treatment with 5'Aza-2'-deoxycytidine was as described (Mavrakis et al., 2008). Whole genome amplified and in vitro methylated DNA served as negative and positive controls, respectively.

HELP (HpaII tiny fragment enrichment by ligation-mediated PCR) assay for DNA methylation. Specimens were obtained from patients with DLBCL in Vancouver at the British Columbia Cancer Agency or Weill Cornell Medical Center. Cases were selected

based on the presence of at least 80% of Lymphoma within the section. The use of human tissue was in agreement with research ethics board of the Vancouver Cancer Center/University of British Columbia and Weill Cornell Medical Center. The HELP assay was performed as previously published (Shaknovich et al., 2010) and using two probes located upstream and overlapping with transcriptional start site of the EphA7 gene. Products of HELP were hybridized to HG_17 human promoter custom array covering 25,626 HpaII amplifiable fragments from Roche NimbleGen, Inc. (Madison, WI). The data quality control (QC) and analysis was performed as described (Thompson et al., 2008). After QC processing, a quintile normalization was performed on each array. Validation of HELP results by Mass Array Pitying MassArray validations were performed on bisulfite converted DNA from the same samples, as were profiled by HELP. Correlation of Massarray results with normalized data from HELP assay revealed R=0.88 (Spearman's correlation). The adjusted linear regression model was used to obtain the conversion formula. Single locus quantitative DNA methylation assays by epityper method (Sequenom, CA) were performed on bisulfite-converted DNA, as previously described. Primers were designed using Sequenom EpiDesigner beta software to cover the outermost HpaII sites of selected HpaII Amplifiable Fragments (HAF), as well as any other HpaII sites found up to 2,000 bp up or downstream form the HAF, in order to cover all possible alternative sites of digestion. The primer sequences are available upon request.

Immunohistochemical and TMA Methods. Tissue microarrays were constructed as previously published (Scott et al., 2007), however, using a fully automated Beecher

Instrument, ATA-27. The study cohort comprised of follicular lymphoma, consecutively ascertained at the Memorial Sloan-Kettering Cancer Center (MSKCC) between 1985 and 2000. Use of tissue samples were approved with an Institutional Review Board Waiver and approval of the Human Biospecimen Utilization Committee. All cancer biopsies were evaluated at MSKCC, and the histological diagnosis was based on haematoxylin and eosin (H&E) staining. TMAs were stained with the EphA7 rabbit polyclonal antibody from Abgent (San Diego, CA), stained on Ventana Discovery XT (Tuscon, AZ), using protocol 67: CC1, standard, at 1:50 dilution for 60 min. then with a secondary anti-rabbit antibody from Vector Labs (Burlingame, CA), at 1:200 dilution for 60 min. Cores were scored as 0, 1, 2 where 0=no staining; 1=focal, weak staining, and 2-moderate to strong staining in more than 50% of tumor cells.

Antibody production and purification. To construct the anti-CD20-EPHA7 antibody, we amplified the EPHA7TR coding sequence by PCR from human genomic DNA. The PCR product has been cloned into the pAH6747 vector containing an IgG1 constant region with an anti-CD20 heavy chain variable region (a generous gift from Dr. Sherie Morrison, UCLA). For antibody production the heavy and light chain vectors (pAG10818) were transiently transfected in 293T cells and the media in which the cells were growing was replaced every other day. CD20-Epha7 was purified from this conditioned media via affinity chromatography using rProtein A. Briefly, the harvested media containing CD20-EphA7 was dialyzed into 20 mM Sodium Phosphate (pH 7), passed over a 1 ml Hitrap rProtein A FF column (GE Life Sciences – 17-5079-02) and eluted with 100mM Glycine-HCl (pH 2.7). Eluant was immediately neutralized with 75 ul 1M Tris-HCl (pH 9.0) / ml eluant as it was collected into glass fraction tubes. The

antibody peak was pooled, dialyzed into PBS and sterile filtered. Purity was determined by SDS-PAGE and antibody-fusion product concentration determined with a spectrophotometer (280 nm) using an extinction coefficient of 1.43. ELISA assay was used to verify protein purity and integrity, using anti-human-IgG (H+L) (Jackson cat. 709-005-149) and HRP-anti-Human Fc (Jackson cat 709-035-098) antibodies.

Cell culture, viability, proliferation assays and vectors and pooled shRNA library screen. FL5-12 murine lymphocytes were stably transduced with Bcl2 (FL5-12/Bcl2); IL3 depletion studies and viral transductions were as described (Mavrakis et al., 2008). Cell death assays based on uptake of DNA staining dye (LDS751) using Viacount assays from Guava Technologies performed as reported (Mavrakis et al., 2008). The retroviral vectors are based on MSCV, and include Bcl2 (Wendel et al., 2004), and individual or pooled shRNA vectors (Dickins et al., 2005). Pooled shRNA screening technology has been described (Mavrakis et al., 2010). Briefly, the shRNA library was constructed by pooling the individually cloned shRNAs **(Table S7).** The screen design is depicted in Figure 2a. Briefly FL5-12/Bcl2 cells were transduced at low multiplicity of infection with the library pool containing 262 shRNAs and subjected to 7d IL3 depletion. Samples were collected after viability had recovered for DNA isolation. Integrated shRNAs were amplified by PCR, subcloned into the pGEM-T vector (Promega, A1360) and identified by shRNA sequencing. Individual 'hits' from the screen were re-tested in the same *in vitro* assay, and confirmed using multiple shRNAs against the same genes. The shRNAs against *Pten* and *p53* have been reported (Mavrakis et al., 2010; Wendel et al., 2006).

Generation of mice. The *vavPBcl2* mouse model of FL is described (Egle et al., 2004) and adapted to adoptive transfer of retrovirally transduced HPCs (Wendel et al., 2004). Data were analyzed in Kaplan-Meier format using the log-rank (Mantel-Cox) test for statistical significance. H&E, Ki67, TUNEL, cleaved caspase, and B220 stains, and surface marker analysis were as in (Mavrakis et al., 2008). Xenografts were by s.c. injection of 1 Mio Raji or SU-DHL-10 human lymphoma cells mixed with matrigel (BD Bioscience, 354230) into the flanks of mice NOD/SCID (NOD.CB17-*Prkdc*^{scid}/J). Upon tumor size > 1cm^3 mice were treated by three intra tumoral injections of vehicle or 20µg EPHA7^{FC} (a purified, truncated, FC-tagged EPHA7^{TR} was from R&D System, 608A7-200). Tumors were weighed and volumes were measured as in (Bergers et al., 1999). Systemic application of EPHA7 and anti-CD20-EPHA7 was by tail vein injection and dosed as described in the results section.

Western blot analysis, ELISA, and protein arrays. Immunoblots were performed from whole cell lysates or supernatant as described (Wendel et al., 2004). Briefly, 50µg of protein/sample were resolved on SDS-PAGE gels and transferred to Immobilon-P-membranes (Millipore). Antibodies were against EphA7 (sc917 1:200 Santa Cruz), EphA2 (clone D7 Millipore cat #05-480 1:1000), Bcl2 (sc509 1:500 Santa Cruz), c-Myc (sc40 1:200 Santa Cruz), phosphorylated eIF4E-BP1 (9451 1:1000 Cell Signaling), phosphorylated Erk1/2 (9101 1:800 Cell signaling), Erk1/2 (9102 1:1000 Cell Signaling), phosphorylated Src (2101 1:1000 Cell signaling), phosphorylated S6 (2215, 1:1000, Cell Signaling), phosphorylated Akt (4058, 1:1000, Cell Signaling), Tubulin (1:5000; Sigma, B-5-1-2). Enhanced chemiluminescence was used for detection (ECL, Amersham). The

human phospho-protein array (R&D Systems, ARY003) and probed with lysates according to manufacturer instructions, the full list of proteins is available upon request and from the manufacturer's website**.** ELISA Assay: The DuoSet IC Elisa human Phospho-Epha2 (R&D DYC4056-2) was performed with whole Raji cell lysates according to manufacturer instructions.

Production of EphA7^{FC} protein. In addition to the commercial protein (R&D System, 608A7-200), we produced an identical protein including the extracellular domain (ECD) of mouse EphA7 using a baculoviral expression system. A fragment corresponding to residues Lys-31 till Asn-525 was cloned using the BamH1/Not1 sites of the pAcGP67B-based (PharMingen) pMA152, a self-made baculovirus vector with Fc-tag at the C-terminus (18,19). The recombinant baculovirus vectors were co-transfected with BaculoGold DNA (PharMingen) in SF9 cells. Passage 4 was used to infect Hi5 cells in suspension at a density of $1.8x10^6$ cells/ml in sf-900 SFM (GIBCO). Infected cells were grown at 27^oC and 100 rpm and harvested after 64 hours. Supernatant of Hi5 cells (4 liters) containing the secreted EphA7-ECD was loaded on ProteinA Sepharose column and eluted by a step-wise pH gradient of 100 mM Glycine. After Fc-tag cleavage by thrombin, proteins were again loaded on ProteinA Sepharose column and flow throw was collected. Gel filtration was used to get monomeric and/or dimeric forms of the protein of interest. The yield was 1-2 mg protein per liter of Hi5 cells suspension (Antipenko et al., 2003; Xu et al., 2008).

Real time quantitative PCR. Total RNA was extracted from tumor samples and cell lines using the Allprep DNA/RNA/Protein. cDNA synthesis and qRT-PCR and analysis by the ΔΔ Ct method as described (Mavrakis et al., 2008). Taqman Gene Expression Assays: Gusb (4333767F, Applied Biosystems) and Sybr green assay Epha7 (primerF TTTCAAACTCGGTACCCTTCA, PrimerR CATTGGGTGGAGAGGAAATC) and Gapdh (PrimerF GAGTCAACGGATTTGGTCGT, primerR GACAAGCTTCCCGTTCTCAG). The purified normal B-cell subsets form tonsil and tumor cells form FL specimens was obtained form the laboratory of Riccardo Dalla-Favera (Columbia University, NY).

PCR amplification and sequencing. Performed as in (Veeriah et al., 2010). In detail, the exonic regions of interest (NCBI Human Genome Build 36.1) were broken into amplicons of 500 bp or less, and specific primers were designed using Primer 3, to cover the exonic regions plus at least 50 bp of intronic sequences on both sides of intron-exon junctions. M13 tails were added to facilitate Sanger sequencing. PCR reactions were carried out in 384 well plates, in a Duncan DT-24 water bath thermal cycler, with 10 ng of whole genome amplified DNA (Repli-G Midi, Qiagen) as template, using a touchdown PCR protocol with HotStart Taq (Kapa Biosystems, SA). The touchdown PCR method consisted of: 1 cycle of 95°C for 5 min; 3 cycles of 95°C for 30 sec, 64°C for 30 sec, 72°C for 60 sec; 3 cycles of 95°C for 30 sec, 62°C for 30 sec, 72°C for 60 sec; 3 cycles of 95°C for 30 sec, 60°C for 30 sec, 72°C for 60 sec; 37 cycles of 95°C for 30 sec, 58°C for 30 sec, 72°C for 60 sec; 1 cycle of 70°C for 5 min. Templates were purified using AMPure (Agencourt Biosciences). The purified PCR reactions were split into two, and

sequenced bidirectionally with M13 forward and reverse primer and Big Dye Terminator Kit v.3.1 (Applied Biosystems). Dye terminators were removed using the CleanSEQ kit (Agencourt Biosciences), and sequence reactions were run on ABI PRISM 3730xl sequencing apparatus (Applied Biosystems).

Mutation detection. Mutations were detected using an automated detection pipeline at the MSKCC Bioinformatics Core. Bi-directional reads and mapping tables (to link read names to sample identifiers, gene names, read direction, and amplicon) were subjected to a QC filter which excludes reads that have an average phred score of < 10 for bases 100-200. Passing reads were assembled against the reference sequences for each gene, containing all coding and UTR exons including 5Kb upstream and downstream of the gene, using command line Consed 16.0 (Gordon et al., 1998). Assemblies were passed on to Polyphred 6.02b (Nickerson et al., 1997), which generated a list of putative candidate mutations, and to Polyscan 3.0 (Chen et al., 2007) which generated a second list of putative mutations. The lists were merged together into a combined report, and the putative mutation calls were normalized to '+' genomic coordinates and annotated using the Genomic Mutation Consequence Calculator. The resulting list of annotated putative mutations was loaded into a Postgres database along with select assembly details for each mutation call (assembly position, coverage, and methods supporting mutation call). To reduce the number of false positives generated by the mutation detection software packages, only point mutations which are supported by at least one bi-directional read pair and at least one sample mutation called by Polyphred were considered, and only the putative mutations which are annotated as having non-synonymous coding effects, occur

within 11 bp of an exon boundary, or have a conservation score > 0.699 (http://genome.ucsc.edu/cgi-bin/hgTrackUi?hgsid=108554407&g=multiz17way) were included in the final candidate list. Indels called by any method were manually reviewed and included in the candidate list if found to hit an exon. All putative mutations were confirmed by a second PCR and sequencing reaction, in parallel with amplification and sequencing of matched normal tissue DNA. All traces for mutation calls were manually reviewed.

Supplemental References.

Antipenko, A., Himanen, J.P., van Leyen, K., Nardi-Dei, V., Lesniak, J., Barton, W.A., Rajashankar, K.R., Lu, M., Hoemme, C., Puschel, A.W.*, et al.* (2003). Structure of the semaphorin-3A receptor binding module. Neuron *39*, 589-598.

Bergers, G., Javaherian, K., Lo, K.M., Folkman, J., and Hanahan, D. (1999). Effects of angiogenesis inhibitors on multistage carcinogenesis in mice. Science *284*, 808-812.

Chen, K., McLellan, M.D., Ding, L., Wendl, M.C., Kasai, Y., Wilson, R.K., and Mardis, E.R. (2007). PolyScan: an automatic indel and SNP detection approach to the analysis of human resequencing data. Genome Res *17*, 659-666.

Dickins, R.A., Hemann, M.T., Zilfou, J.T., Simpson, D.R., Ibarra, I., Hannon, G.J., and Lowe, S.W. (2005). Probing tumor phenotypes using stable and regulated synthetic microRNA precursors. Nat Genet *37*, 1289-1295.

Egle, A., Harris, A.W., Bath, M.L., O'Reilly, L., and Cory, S. (2004). VavP-Bcl2 transgenic mice develop follicular lymphoma preceded by germinal center hyperplasia. Blood *103*, 2276-2283.

Gordon, D., Abajian, C., and Green, P. (1998). Consed: a graphical tool for sequence finishing. Genome Res *8*, 195-202.

Himanen, J.P., Henkemeyer, M., and Nikolov, D.B. (1998). Crystal structure of the ligand-binding domain of the receptor tyrosine kinase EphB2. Nature *396*, 486-491.

Mandelbaum, J., Bhagat, G., Tang, H., Mo, T., Brahmachary, M., Shen, Q., Chadburn, A., Rajewsky, K., Tarakhovsky, A., Pasqualucci, L.*, et al.* (2010). BLIMP1 Is a Tumor Suppressor Gene Frequently Disrupted in Activated B Cell-like Diffuse Large B Cell Lymphoma. Cancer Cell *18*, 568-579.

Mavrakis, K.J., Wolfe, A.L., Oricchio, E., Palomero, T., de Keersmaecker, K., McJunkin, K., Zuber, J., James, T., Khan, A.A., Leslie, C.S.*, et al.* (2010). Genome-wide RNA-mediated interference screen identifies miR-19 targets in Notch-induced T-cell acute lymphoblastic leukaemia. Nat Cell Biol *12*, 372-379.

Mavrakis, K.J., Zhu, H., Silva, R.L., Mills, J.R., Teruya-Feldstein, J., Lowe, S.W., Tam, W., Pelletier, J., and Wendel, H.G. (2008). Tumorigenic activity and therapeutic inhibition of Rheb GTPase. Genes Dev *22*, 2178-2188.
McBride, K.M., Gazumyan, A., Woo, E.M., Schwickert, T.A., Chait, B.T., and Nussenzweig, M.C. (2008). Regulation of class switch recombination and somatic mutation by AID phosphorylation. J Exp Med *205*, 2585-2594.
Nickerson, D.A., Tobe, V.O., and Taylor, S.L. (1997). PolyPhred: automating the detection and genotyping of single nucleotide substitutions using fluorescence-based resequencing. Nucleic Acids Res *25*, 2745-2751.
Scott, C.L., Gil, J., Hernando, E., Teruya-Feldstein, J., Narita, M., Martinez, D., Visakorpi, T., Mu, D., Cordon-Cardo, C., Peters, G.*, et al.* (2007). Role of the chromobox protein CBX7 in lymphomagenesis. Proc Natl Acad Sci U S A *104*, 5389-5394.
Shaknovich, R., Figueroa, M.E., and Melnick, A. (2010). HELP (HpaII tiny fragment enrichment by ligation-mediated PCR) assay for DNA methylation profiling of primary normal and malignant B lymphocytes. Methods Mol Biol *632*, 191-201.
Thompson, R.F., Reimers, M., Khulan, B., Gissot, M., Richmond, T.A., Chen, Q., Zheng, X., Kim, K., and Greally, J.M. (2008). An analytical pipeline for genomic representations used for cytosine methylation studies. Bioinformatics *24*, 1161-1167.
Veeriah, S., Taylor, B.S., Meng, S., Fang, F., Yilmaz, E., Vivanco, I., Janakiraman, M., Schultz, N., Hanrahan, A.J., Pao, W.*, et al.* (2010). Somatic mutations of the Parkinson's disease-associated gene PARK2 in glioblastoma and other human malignancies. Nat Genet *42*, 77-82.
Wendel, H.G., de Stanchina, E., Cepero, E., Ray, S., Emig, M., Fridman, J.S., Veach, D.R., Bornmann, W.G., Clarkson, B., McCombie, W.R.*, et al.* (2006). Loss of p53 impedes the antileukemic response to BCR-ABL inhibition. Proc Natl Acad Sci U S A *103*, 7444-7449.
Wendel, H.G., De Stanchina, E., Fridman, J.S., Malina, A., Ray, S., Kogan, S., Cordon-Cardo, C., Pelletier, J., and Lowe, S.W. (2004). Survival signalling by Akt and eIF4E in oncogenesis and cancer therapy. Nature *428*, 332-337.
Xu, K., Rajashankar, K.R., Chan, Y.P., Himanen, J.P., Broder, C.C., and Nikolov, D.B. (2008). Host cell recognition by the henipaviruses: crystal structures of the Nipah G attachment glycoprotein and its complex with ephrin-B3. Proc Natl Acad Sci U S A *105*, 9953-9958.
Yu, D., and Thomas-Tikhonenko, A. (2002). A non-transgenic mouse model for B-cell lymphoma: in vivo infection of p53-null bone marrow progenitors by a Myc retrovirus is sufficient for tumorigenesis. Oncogene *21*, 1922-1927.

Suppl. Figure 1

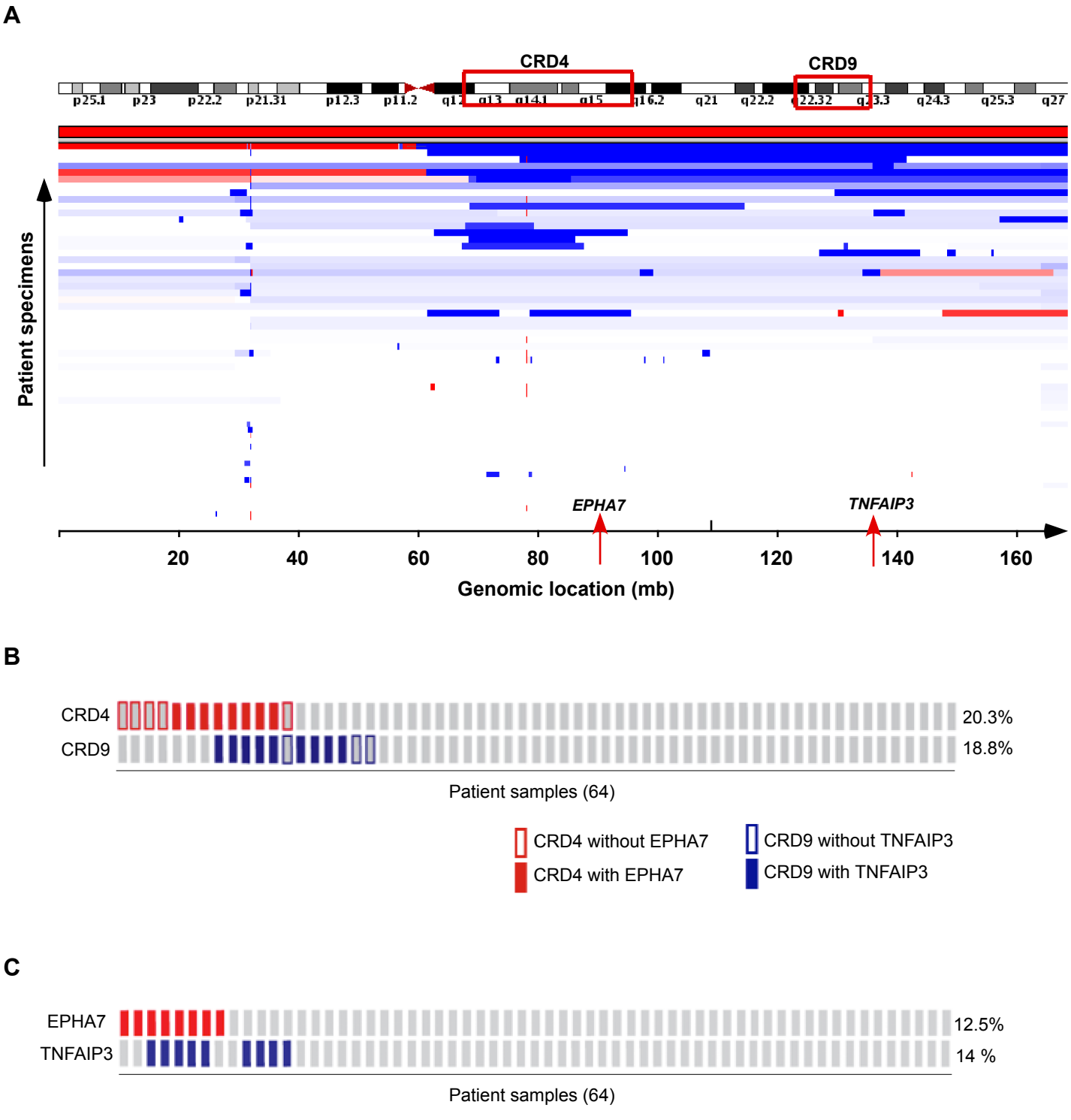

Suppl. Fig. 2

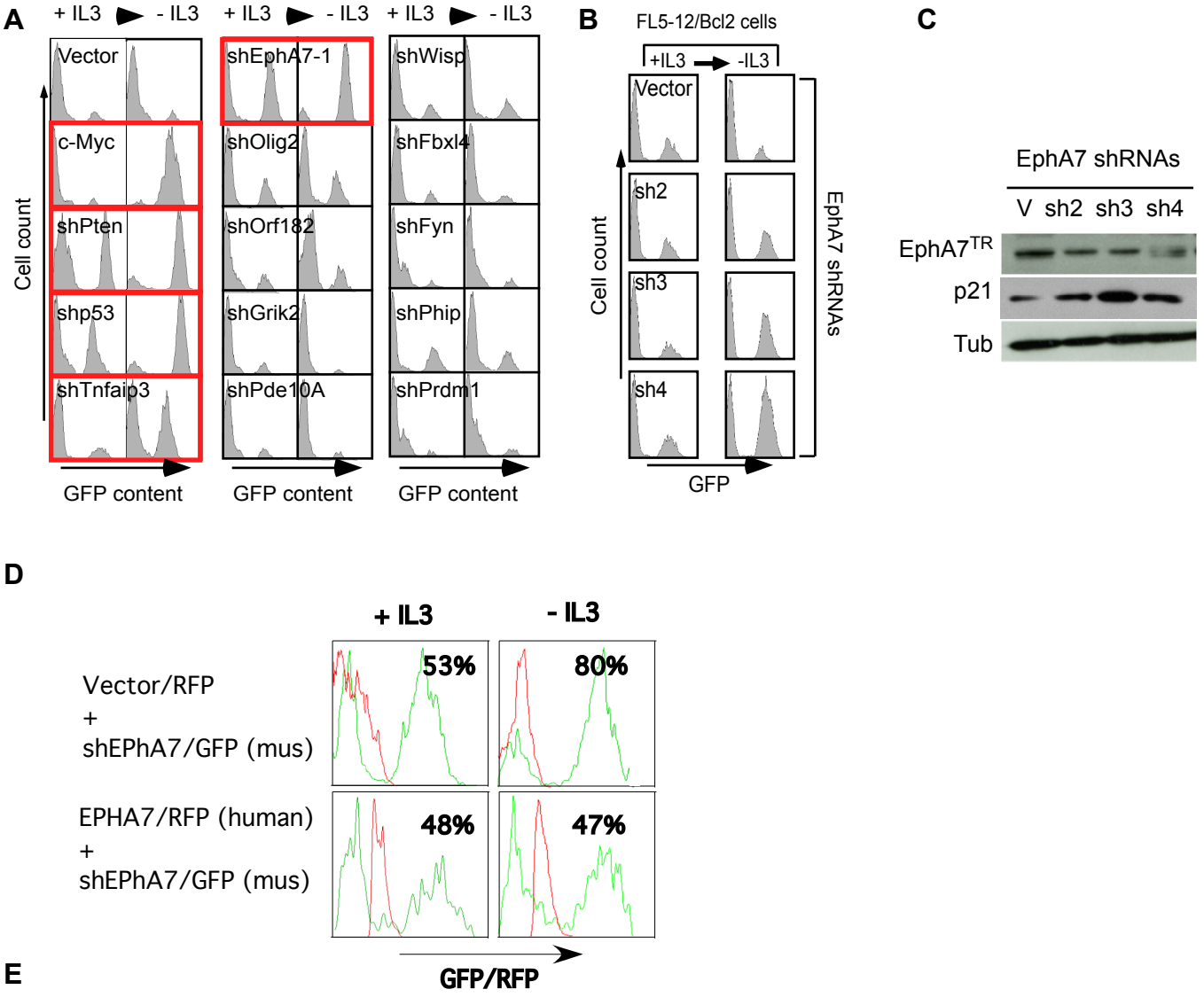
A
+ IL3
- IL3
Vector
c-Myc
shPten
shp53
shTnfaip3
shEphA7-1
shOlig2
shOrf182
shGrik2
shPde10A
shWisp
shFbxl4
shFyn
shPhip
shPrdm1
Cell count
GFP content
B
FL5-12/Bcl2 cells
+IL3
-IL3
Vector
sh2
sh3
sh4
Cell count
GFP
EphA7 shRNAs
C
EphA7 shRNAs
V sh2 sh3 sh4
EphA7TR
p21
Tub
D
+ IL3
- IL3
Vector/RFP
+
shEPhA7/GFP (mus)
53%
80%
EPHA7/RFP (human)
+
shEPhA7/GFP (mus)
48%
47%
GFP/RFP
E
shEphA7
Vector
% cells / cell cycle phase
100
80
60
40
20
0
G2/M
S
G1
t=0
-IL3/48h
+IL3/1h
+IL3/2h
+IL3/3h
+IL3/6h

Suppl. Fig. 3

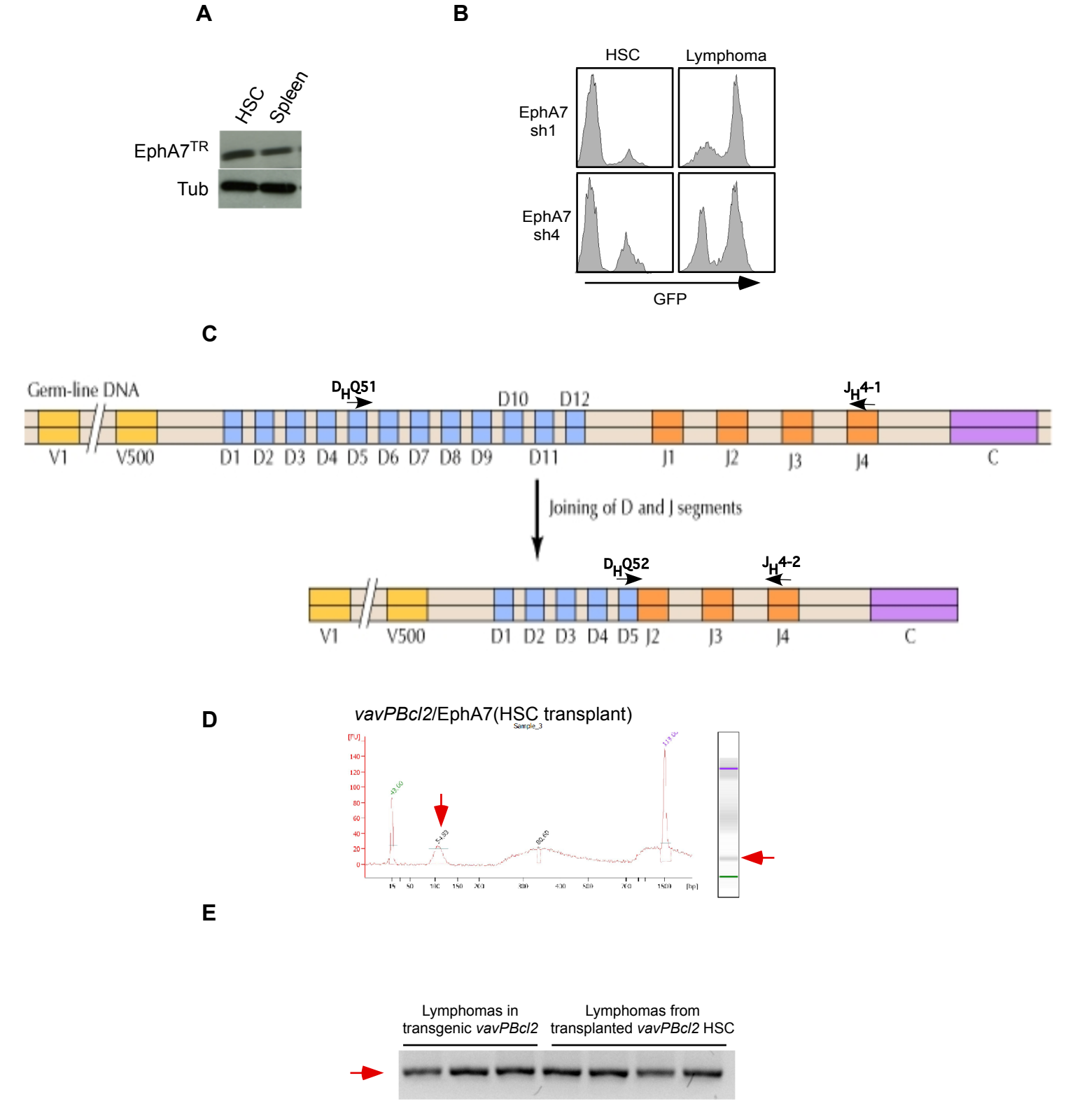
A
HSC
Spleen
EphA7TR
Tub
B
HSC
Lymphoma
EphA7 sh1
EphA7 sh4
GFP
C
Germ-line DNA
DHQ51
D10
D12
JH4-1
V1
V500
D1
D2
D3
D4
D5
D6
D7
D8
D9
D11
J1
J2
J3
J4
C
Joining of D and J segments
DHQ52
JH4-2
V1
V500
D1
D2
D3
D4
D5
J2
J3
J4
C
D
vavPBcl2/EphA7(HSC transplant)
E
Lymphomas in transgenic vavPBcl2
Lymphomas from transplanted vavPBcl2 HSC

Supplemental Figure

Suppl. Fig. 4

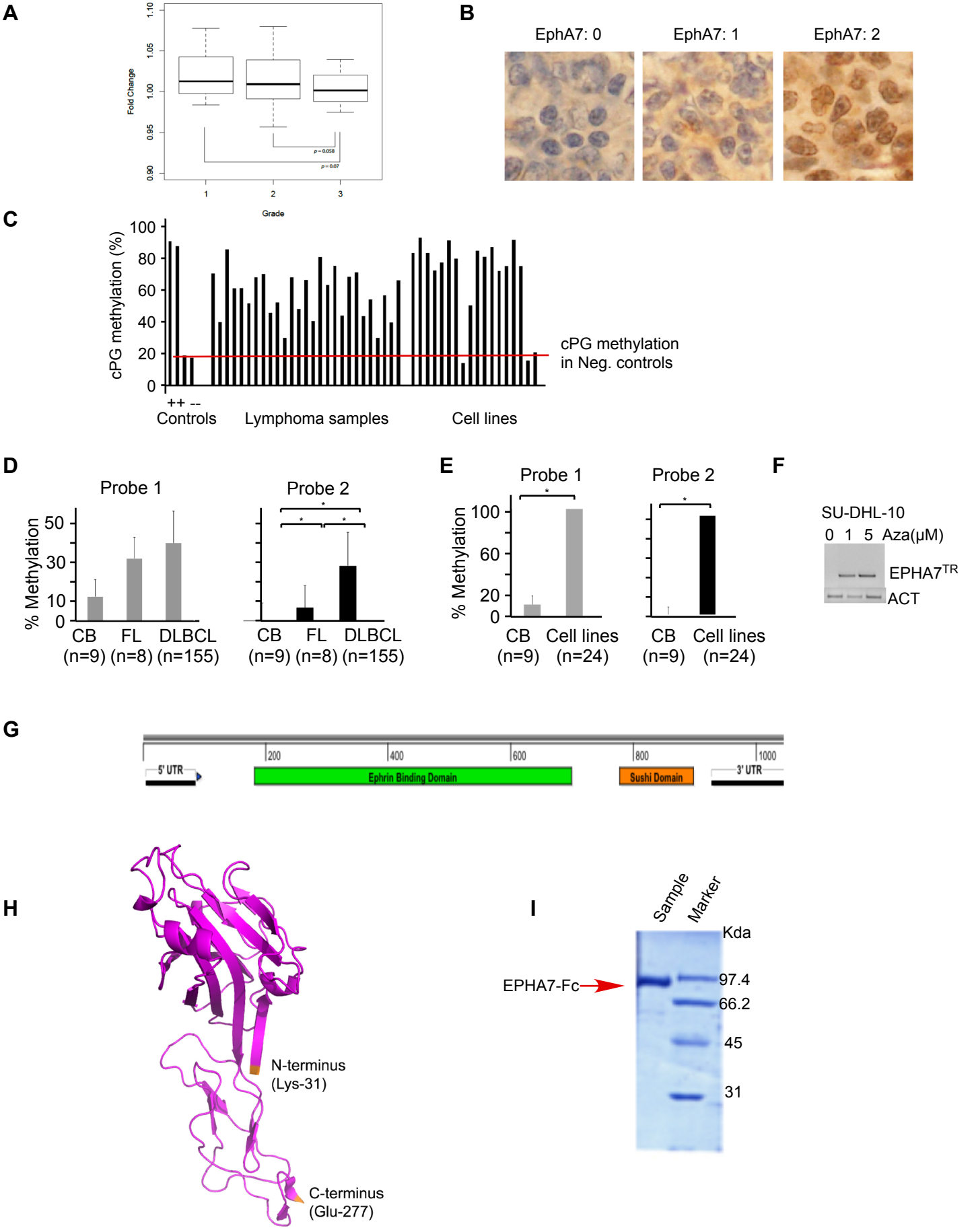

Supplemental Figure

Suppl. Fig. 5

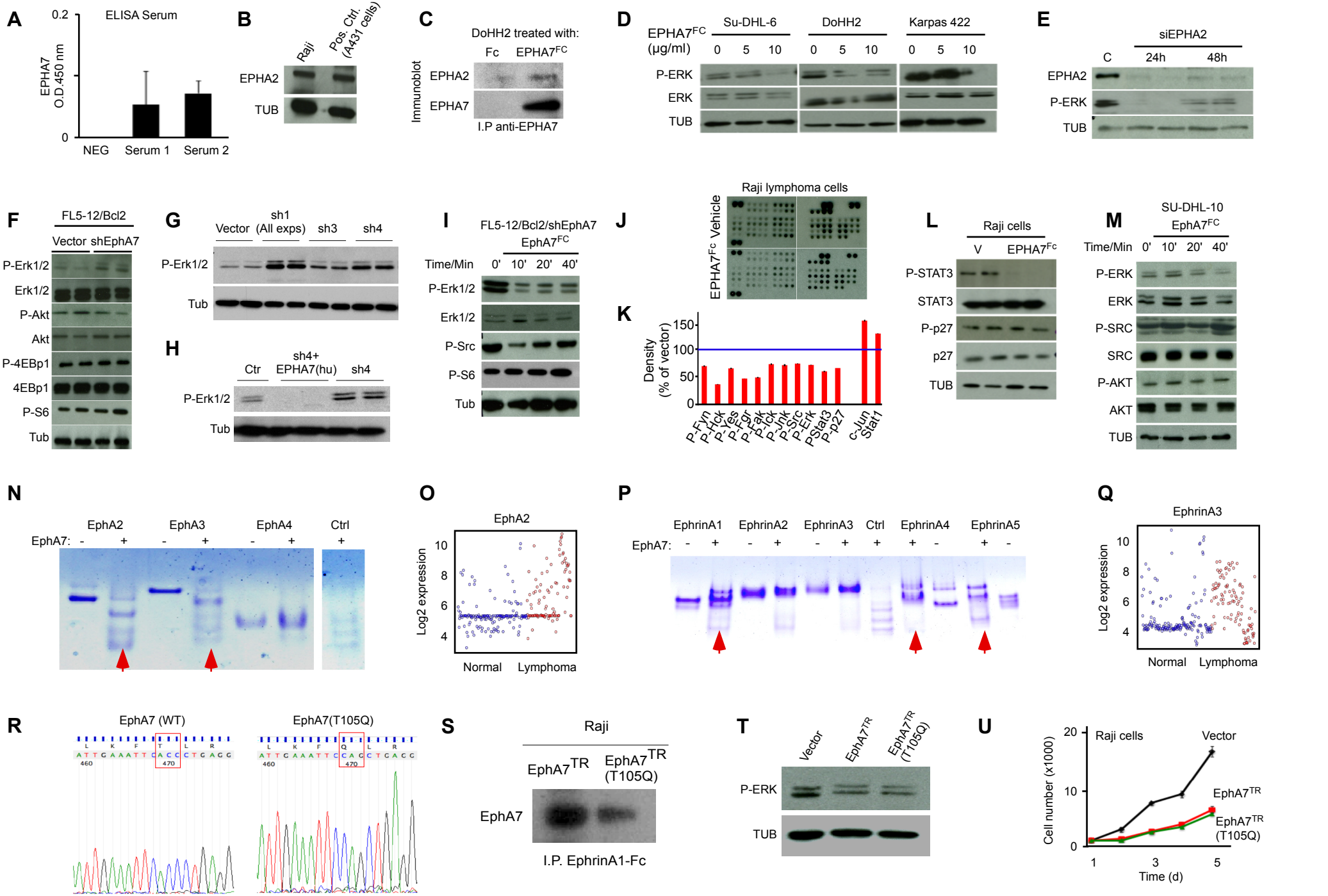

Supplemental Figure

Suppl. Fig. 6

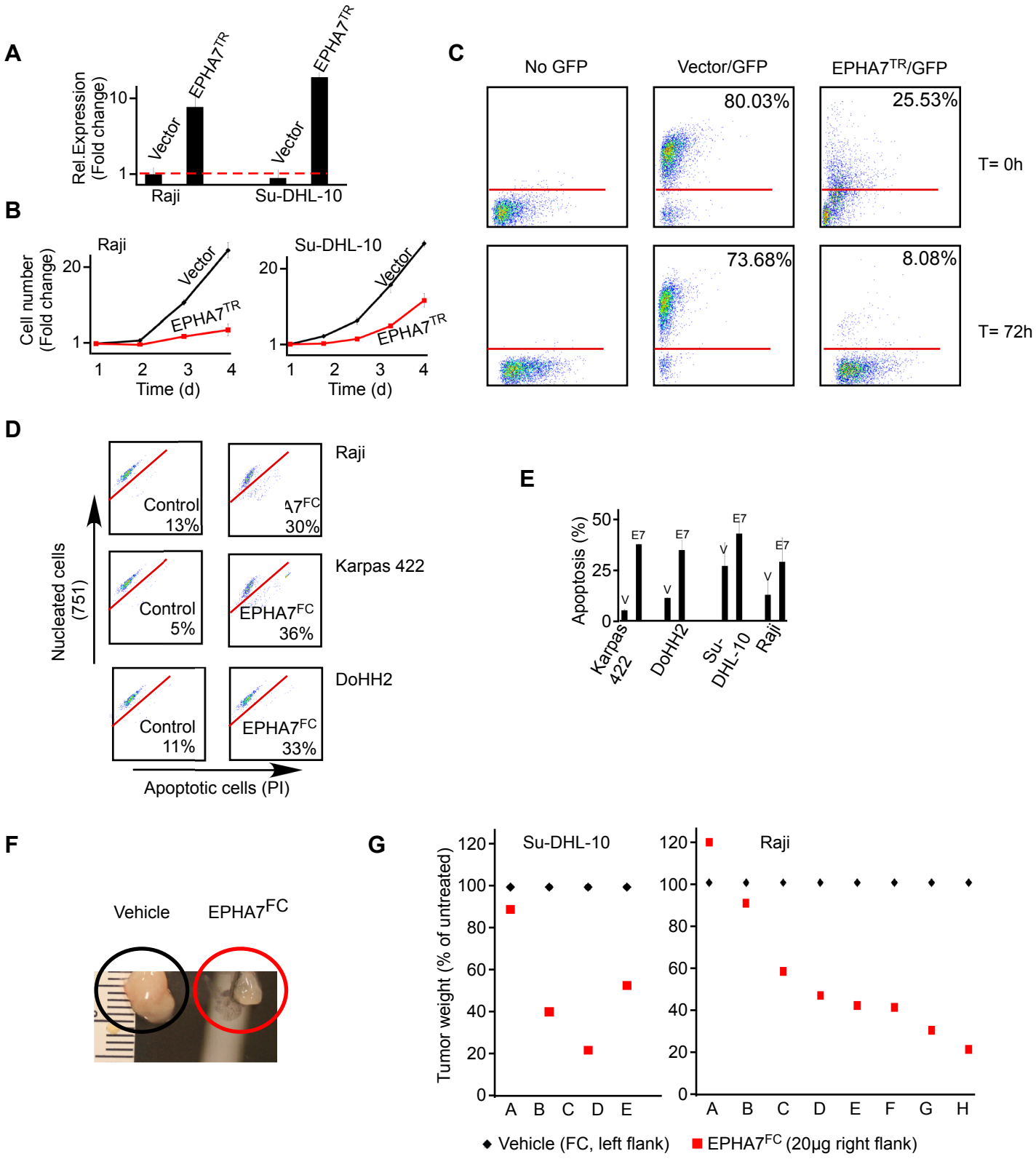

Supplemental Figure

Suppl. Fig. 7